

Influence of barrier and well on the performance $\text{Ge}_{1-y}\text{Sn}_y/\text{Ge}_{1-x}\text{Sn}_x/\text{Ge}_{1-y}\text{Sn}_y$ quantum well for the mid-infrared detector

Omar Zitouni^{1,2}, Nouha Mastour¹ and Said Ridene^{1,*}

¹Advanced Materials and Quantum Phenomena Laboratory, Physics Department, Faculty of Sciences of Tunis, University of Tunis El Manar, Tunis 2092, Tunisia; ozitouni555@gmail.com (O.Z.); mastournouha@yahoo.fr (N.M.)

²Laboratoire Photovoltaïque (LPV)- CRTE n Borj Cédria, Tunis, Tunisia

*Correspondence: author. E-mail Address: said.ridene@fst.rnu.tn

Abstract- This study examines the optical gain and subband states of $\text{Ge}_{1-y}\text{Sn}_y/\text{Ge}_{1-x}\text{Sn}_x/\text{Ge}_{1-y}\text{Sn}_y$ quantum wells (QWs) with different α -Sn concentrations and well widths. Using a 14-band k - p Hamiltonian, we explore various configurations of Sn concentrations in the active region and barrier, revealing that a very low concentration of Sn in the barrier improves carrier confinement in the well, leading to stronger optical gain. The analysis shows that optical gain strongly depends on the α -Sn concentration and the well width. However, as the α -Sn concentration in the barrier increases beyond a certain threshold (around $0.26x$), the optical gain starts to decrease. The study predicts that mid-infrared lasers operating at room temperature could be achieved with optimized $\text{Ge}_{1-y}\text{Sn}_y/\text{Ge}_{1-x}\text{Sn}_x/\text{Ge}_{1-y}\text{Sn}_y$ quantum well structures, where the α -Sn concentrations in the barrier and active region are carefully balanced.

Keywords— Barrier and well influence, GeSn Q-well, optical gain, Mid-infrared laser structures

I. Introduction

Germanium(Ge) and tin (Sn) group-IV materials have attracted considerable attention due to their promising electronic and optical properties [1-4]. The optical characteristics, such as laser activity and optical gain, can be significantly improved when germanium is combined with the semi-metallic α -Sn. In recent years, SiGeSn quantum well (QW) structures have garnered considerable interest in both theoretical and experimental studies [5-8]. However, notable advancements in optoelectronic devices, including infrared photo detectors operating in the terahertz wavelength range, have been achieved with GeSn/SiGeSn [9] or through the optimization of various structural parameters in SiGeSn [10]. Furthermore, the optoelectronic properties of SiGeSn can be greatly enhanced by adjusting the α -Sn concentration, particularly by transition from an indirect to a direct bandgap [11,12].

Experimental work has shown that a direct bandgap structure can be obtained by incorporating a small amount of α -Sn [6], which also leads to a significant increase in photoluminescence intensity. The development and photoluminescence characterization of GeSn have made important contributions to the advancement of Si-based optoelectronics [7,11]. Additionally, several studies have demonstrated that the direct bandgap structure of $\text{Ge}_{1-x}\text{Sn}_x$ can be achieved when $x = 0.12$ [13]. Moreover, due to the tunable bandgap of GeSn, the ternary alloy SiGeSn can exhibit similar inter-band transitions. Experimental and theoretical investigations have shown that SiGeSn offers a broader range of bandgap and lattice variations compared to its binary counterpart, thereby enabling additional applications.

An intriguing aspect of GeSn quantum well (QW) lasers is the threshold carrier densities required for light emission and the underlying physical mechanisms responsible for low-temperature lasing. These factors have been explored in comparison to threshold carrier densities in traditional III-V and II-VI QW lasers [14]. Indeed, lasing in GeSn has been studied, and it has been found that the optical gain emission behavior in GeSn QWs is similar to that observed in II-VI and III-V QWs when n-type doping is introduced at concentrations of

$6 \times 10^{18} \text{ cm}^{-3}$. Additionally, recent theoretical studies have also investigated GeSn quantum dots for potential photo detection applications [15].

Thus, studying the $\text{Ge}_{1-y}\text{Sn}_y/\text{Ge}_{1-x}\text{Sn}_x/\text{Ge}_{1-y}\text{Sn}_y$ alloys becomes increasingly relevant, as it offers a systematic approach to optimize Sn concentration in both optically active layers and electronic confinement layers [3]. These investigations aim to achieve the ultimate goal of a **low-threshold GeSn laser** operating at room temperature, which is a critical milestone for developing integrated photonic solutions with low power consumption and more efficient devices for the microelectronics industry.

To explore the optimal injection carrier density and the concentration of α -Sn in germanium, it is crucial to utilize the 14-band model. This approach allows for the consideration of the effects of distant conduction band (CB) and valence band (VB) levels, which can significantly impact inter-band transitions and the optical gain emission process. Unlike the 8-band $k\cdot p$ model, the 14-band $k\cdot p$ Hamiltonian is more suitable for applications involving high injection carrier densities and doped concentrations. This is due to the inclusion of additional band interactions in the 14-band $k\cdot p$ model, such as the $[(\Gamma_{7C}, \Gamma_{8C})-\Gamma_{6C}]$, $[(\Gamma_{7C}, \Gamma_{8C})-(\Gamma_{7V}, \Gamma_{8V})]$, and $[\Gamma_{6C}-(\Gamma_{7V}, \Gamma_{8V})]$ interactions. These represent the coupling between different conduction bands (CBs), the higher CB with the VB, and the coupling between the lower CB and VB, whereas the 8-band $k\cdot p$ Hamiltonian only considers the interaction between the lower CB and VB.

In this study, we theoretically examine the impact of injection carrier density and α -Sn concentration on the CB and VB band structures, wave functions, and optical gain emission. This analysis is conducted within the framework of the 14-band $k\cdot p$ model, accounting for strain effects and interactions between the CB and VB bands. For the numerical analysis, we employ self-consistent iteration and variational methods [5,18].

II. Theoretical Approach to Optical Gain in $\text{Ge}_{1-y}\text{Sn}_y/\text{Ge}_{1-x}\text{Sn}_x/\text{Ge}_{1-y}\text{Sn}_y$ Quantum Wells for Laser Applications

To investigate optical gain properties, such as injection carrier density and α -Sn concentration, a precise understanding of the subband structure is required. Therefore, the subbands of both the conduction band (CB) and the valence band (VB) of $\text{Ge}_{1-y}\text{Sn}_y/\text{Ge}_{1-x}\text{Sn}_x/\text{Ge}_{1-y}\text{Sn}_y$ quantum wells will be analyzed using the 14-band $k\cdot p$ Hamiltonian, H [5,18]:

$$H = H_{kp} + H_{strain} + V_{VBO}(z) + V_{CBO}(z) \quad (1)$$

where H_{kp} represents the $k\cdot p$ Hamiltonian, H_{strain} the strain Hamiltonian, and $V_{VBO}(z)$ and $V_{CBO}(z)$ are the potential offsets for the valence band (VB) and conduction band (CB), respectively. The band alignment and the CB and VB parameters used in the 14-band $k\cdot p$ model for $\text{Ge}_{1-y}\text{Sn}_y/\text{Ge}_{1-x}\text{Sn}_x/\text{Ge}_{1-y}\text{Sn}_y$ quantum wells are illustrated in Figure 1. The matrix and $\{|J, M_J\rangle$ base are provided in our previous work [2].

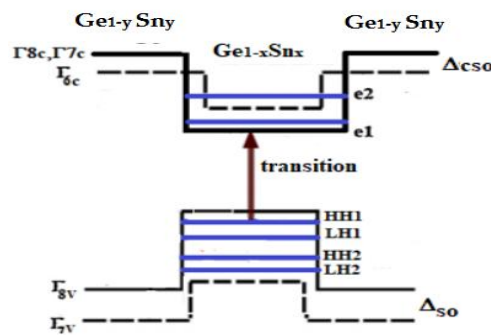


Figure 1. Band configuration of $\text{Ge}_{1-y}\text{Sn}_y/\text{Ge}_{1-x}\text{Sn}_x/\text{Ge}_{1-y}\text{Sn}_y$ quantum wells. Δ_{so} and Δ_{cso} refer to the spin-orbit splitting energies of the conduction and valence bands, respectively.

Concerning the optical gain $g(\omega)$ in quantum wells, it is influenced by the subband structure and is determined by factors such as the 2D density of states ρ_{2D} , the overlap of wave functions, the intra-band relaxation time τ_{in} , and the quasi-Fermi levels f_n^c and f_m^v . Additionally, it depends on the momentum matrix element for optical transitions [16]:

$$g(\omega) = \frac{e^2}{m_0^2 n_r c \epsilon_0 \omega L_{QW}} \frac{1}{\sum_{\sigma=\uparrow, \downarrow} \sum_{nm} J_{cv}^{nm} \int_0^{+\infty} \rho_{2D} |M_{cv}|^2 \left[f(E_{n,k}^c - E_F^c) - f(E_F^v - E_{m,k}^v) \right]} \times \frac{\hbar / \tau_{in}}{\left(\hbar \omega - (E_{n,k}^c - E_{m,k}^v) - E \right)^2 + (\hbar / \tau_{in})^2} dE \quad (2)$$

Where τ_{in} is the intraband relaxation time, which is 10^{-13} s, c is the speed of light, ϵ_0 is the permittivity of free space, e is the electron charge, n_r is the refractive index, L_{QW} refers to the quantum well width and m_0 is the free electron mass.

III. Results and Discussions

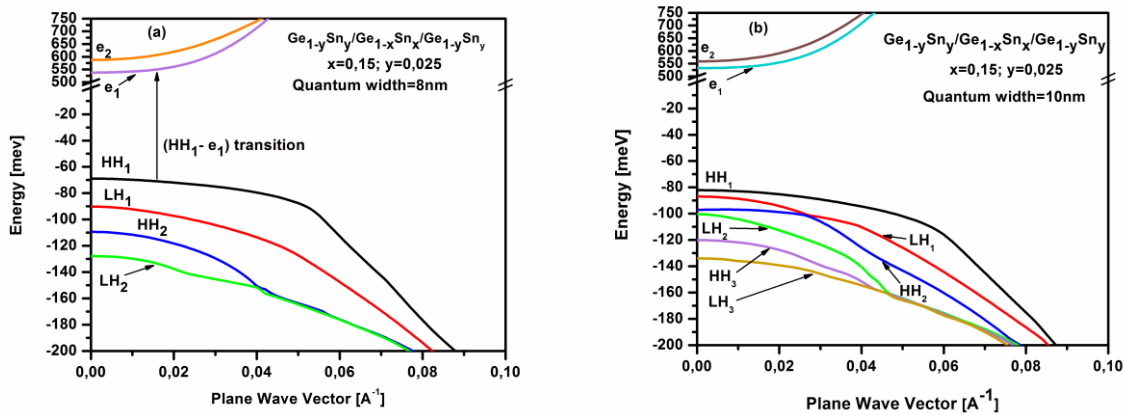
To examine the effect of the quantum well (QW) width and α -Sn concentration, both in the barrier and the active region, on the subband structure and optical gain, we computed the dispersion relation for the conduction band (CB) and valence band (VB) of the $\text{Ge}_{1-y}\text{Sn}_y/\text{Ge}_{1-x}\text{Sn}_x/\text{Ge}_{1-y}\text{Sn}_y$ quantum well, taking into account the α -Sn concentrations and the well width.

We selected the case where $y < x$ (the barrier has a lower Sn concentration than the well): this configuration is expected to provide stronger carrier confinement in the well, which could lead to an increase in optical gain. In contrast, for $y \approx x$, while this could result in a balanced configuration with good carrier confinement, it also causes a reduction in the bandgap.

The case where $y > x$ (the barrier has a higher Sn concentration than the well) is not considered, as it could hinder carrier confinement within the well, reducing optical gain.

The required parameters for Ge and α -Sn used in the numerical calculations are listed in Table 1. The widths of the well and the barrier are approximately (8, 10, 12, 14) nm and 16 nm, respectively, with the energy gap for the well being around 135 meV for heavy HH_n and light LH_n holes [17]. It should be noted that energy is measured in meV, and the reference energy is chosen at the maximum of the unstrained HH_n well. All numerical values for bulk Ge and α -Sn used in this study are sourced from references [17, 18].

Figure 2 illustrates the subband structure of the conduction band (CB) and valence band (VB) of quantum wells with different widths, with fixed Sn concentrations in both the barrier and the active region.



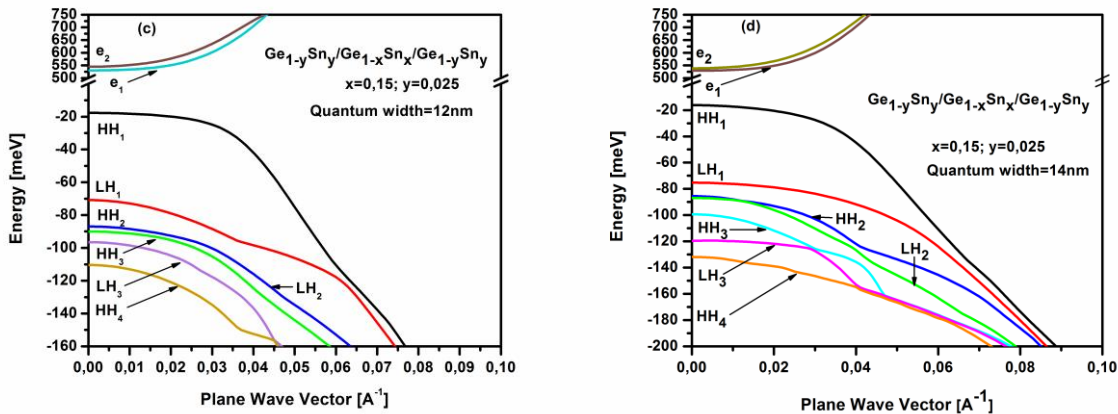
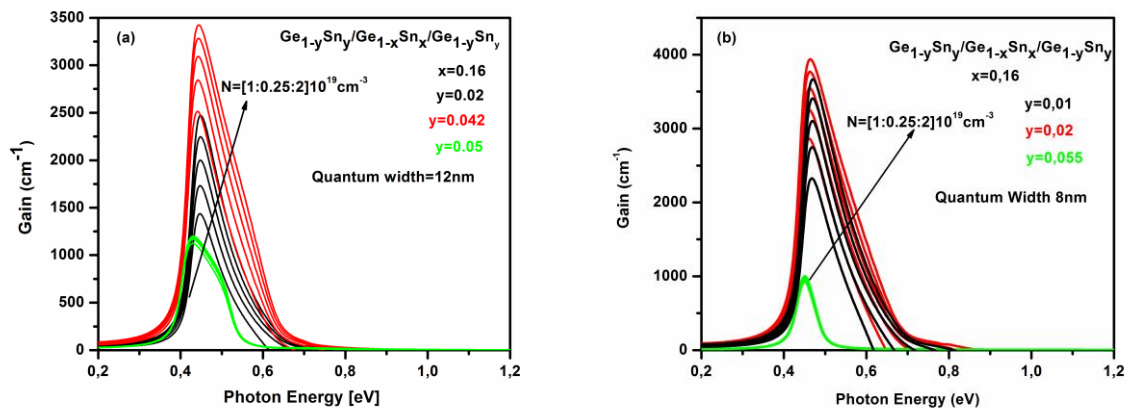


Figure 2 : Subband structure of the conduction band (CB) and valence band (VB) of the $Ge_{1-y}Sn_y/Ge_{1-x}Sn_x/Ge_{1-y}Sn_y$ QW for different widths (8, 10, 12, and 14 nm), calculated for fixed α -Sn concentrations ($y=0.025; =0.15$).

The (HH_n, LH_n, and e_n) correspond to the subbands of holes and electrons in the conduction band (CB) and valence band (VB) for different quantum well widths. For each behavior, marked non-parabolicities are observed due to the mixing of HH_n and LH_n states in the VB. Indeed, strong coupling between the HH_n and LH_n states has been demonstrated. This reality suggests that the VB states are strongly interdependent, both among themselves and with the two CB subbands, in the $Ge_{1-y}Sn_y/Ge_{1-x}Sn_x/Ge_{1-y}Sn_y$ quantum well.

It is worth noting that the number of confined states increases with the quantum well width, as does the difference between the HH_n and LH_n subbands, except for the 10 nm wide well. In contrast, the difference between the first conduction levels (e₁ and e₂) decreases significantly as the well width increases (see Fig. 2(d)). This phenomenon could lead us, in future work, to also consider the HH₁ → e₂ transitions in this type of alloy.

On the other hand, from figure 2, it can be seen that the HH₁ and HH₂ states shift upward, while the LH₁ states shift downward as the well width increases. This can be attributed to the influence of the well width on the energy band gap [9], which may explain the high energy level, as shown in Fig. 2(d). Additionally, the HH₁ → e₁ transition energy is highly dependent on the well width and shifts toward lower energies. This behavior will influence the variation of the optical gain. Optical gain emission as a function of QW width (8nm for α -Sn concentrations ($x=0.16; y=0.01, 0.02, 0.055$) and (12 nm for α -Sn concentrations ($(x=0.16; y=0.02, 0.042, 0.05), (x=0.12; y=0.02, 0.042, 0.043, 0.044), (x=0.1; y=0.01, y=0.02, y=0.026)$ in the $Ge_{1-y}Sn_y/Ge_{1-x}Sn_x/Ge_{1-y}Sn_y$ QWs are presented in figure 3 (a, b, c, d).



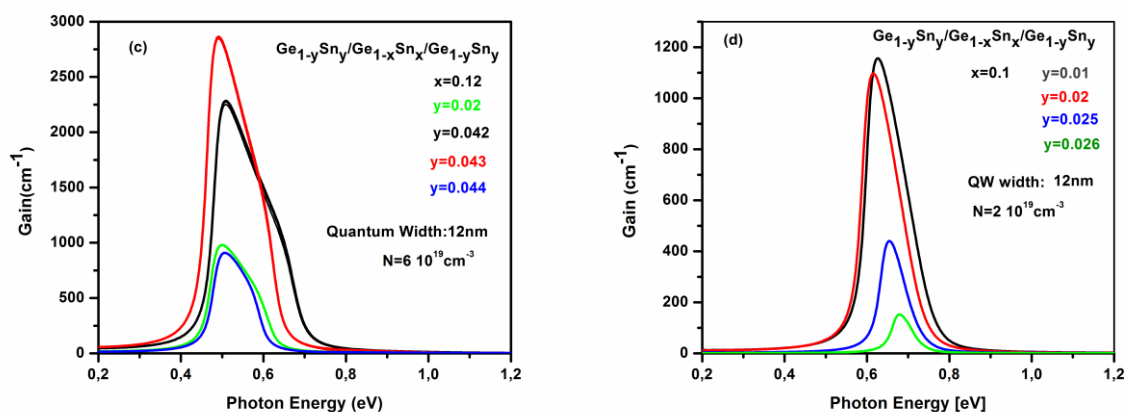


Figure 3. Optical gain as a function of photon energy in Ge_{1-y}Sn_y/Ge_{1-x}Sn_x/Ge_{1-y}Sn_y QWs, calculated: (a-b) for varying carrier injection densities (N) and α -Sn concentrations, with black, red and green arrows indicating the increase in carrier injection densities N [1:0.25:2] × 10¹⁹ cm⁻³. (b-d) are calculated for a typical injected carrier density of 6 × 10¹⁹ cm⁻³ and 12 nm QW width."

It is observed that the optical gain curves exhibit a strong dependence on both the α -Sn concentration and the QW width.

It has been observed that the optical gain curves strongly depend on the α -Sn concentration and the quantum well (QW) width. Notably, for α -Sn concentrations in the barrier ranging from $x = 0.01$ to $x = 0.055$, the peak optical gain remains around 0.4 eV (figures a and b) when a fixed concentration of α -Sn is present in the active region. However, as this concentration in the active region decreases, the emission shifts towards approximately 0.5 eV and beyond (figures c and d). These results suggest that a mid-infrared laser structure operating at room temperature could be achieved with a Ge_{1-y}Sn_y/Ge_{1-x}Sn_x/Ge_{1-y}Sn_y structure with quantum wells (QWs).

In figures c and d, it is observed that as the tin concentration increases, the optical gain increases, but from a value of $y = 0.043$ for $x = 0.12$ with a well width of 12 nm, the gain begins to decline. Similarly, for $x = 0.1$ and a well width of 12 nm, the concentration of y at which the gain decreases is approximately 0.025. This phenomenon may be due to a reduction in the mobility of electrons and holes. Indeed, the addition of Sn introduces perturbations in the crystal structure of Ge, which can lead to an increase in carrier scattering. When carriers (electrons and holes) move less efficiently, the recombination probability decreases, which may reduce the optical gain. Furthermore, increasing the Sn concentration reduces the material's bandgap, which alters the characteristics of electronic transitions. Although this initial reduction may promote optical transitions, an excessive reduction of the bandgap can make these transitions less efficient, as the photon energy becomes too low to effectively excite carriers into the conduction states. This could also reduce the efficiency of optical absorption and emission, thereby contributing to the decrease in optical gain.

In Figure 4, we plotted the optical gain emission for a quantum well width of 12 nm, with y fixed at 0.02 and x varying from 0.1 to 0.16.

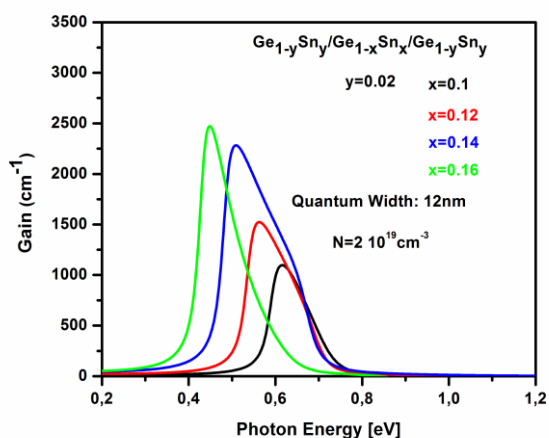


Figure 4. Optical gain versus photon energy in $Ge_{1-y}Sn_y/Ge_{1-x}Sn_x/Ge_{1-y}Sn_y$ QW (Width :12nm) calculated with y fixed at 0.02 and x varying from 0.1 to 0.16, for typical injected carrier density ($2 \times 10^{19} cm^{-3}$).

As x increases while keeping y constant, the gain increases, and the gain peak shifts from 0.63 to 0.4 eV, suggesting that as x increases, the material becomes more suitable for optical transitions in the longer wavelength range. These transitions are more efficient at lower energies, leading to an increase in optical gain and a shift of the peak to longer wavelengths.

IV. Conclusion

Using the 14-band $k \cdot p$ Hamiltonian, we have calculated the subband states of electrons and holes as well as the optical gain of $Ge_{1-y}Sn_y/Ge_{1-x}Sn_x/Ge_{1-y}Sn_y$ quantum wells (QWs) for different α -Sn concentrations and quantum well widths. The results of this study show that the $Ge_{1-y}Sn_y/Ge_{1-x}Sn_x/Ge_{1-y}Sn_y$ quantum well structure with varying α -Sn concentrations in both the well and the barrier has a significant impact on optical gain and carrier confinement properties.

The results also revealed a strong dependence of the optical gain on the quantum well width and α -Sn concentration. An increase in the well width generally improves the confinement of states and the energy gap between the HH_n and LH_n subbands, which can have implications for optimizing optical transitions. However, beyond a certain Sn concentration threshold (e.g., for $x=0.12$ and $y \approx 0.043$), a decrease in optical gain was observed, likely due to crystal lattice perturbations and increased carrier scattering.

In conclusion, to achieve optimal optical gain in $Ge_{1-y}Sn_y/Ge_{1-x}Sn_x/Ge_{1-y}Sn_y$ quantum well structures at room temperature, it is preferable to use low α -Sn concentrations in the barrier and moderate concentrations in the well. These results pave the way for mid-infrared laser structures at room temperature, with potential applications in optoelectronic devices.

References

1. Marzban. B, Stange. D, Rainko. D, Ikonc. Z, Buca. D, J. Witzens. Modeling of a SiGeSn quantum well laser. *Photonics Research* 2021, 9, 1234. <https://doi.org/10.1364/PRJ.416505>.
2. Omar Zitouni, Nouha Mastour, Said Ridene, *Electronics* 2024, 13(21), 4142; <https://doi.org/10.3390/electronics13214142>
3. Q UANG M INH THAI ; NICOLAS PAUC ; JORIS A UBIN ; M ATHIEU BERTRAND ; JÉRÉMIE CHRÉTIEN ; VINCENT DELAYE ; ALEXEI CHELNOKOV ; JEAN-M ICHÉL HARTMANN ; VINCENT R EBOUD AND VINCENT C ALVO Vol. 26, No. 25 | 10 Dec 2018 | OPTICS EXPRESS 32500
4. Junkin.T.M, Harpt. B, Feng. Y, Losert.M.P, Rahman. R, Dodson. J.P, Wolfe.M.A, Savage.D.E, Lagally.M.G, Coppersmith.S.N, Friesen. M, Joynt.R, Eriksson. M.A. SiGe quantum wells with oscillating Ge concentrations for quantum dot qubits. *Nat. Commun.* 2022, 13, 7777. <https://doi.org/10.1038/s41467-022-35510-z>
5. Ridene. S, Boujdaria. K, Bouchriha. H, Fishman. G. Infrared absorption in $Si_{1-x}Ge_x$ quantum wells. *Phys. Rev. B.* 2001, 64, 085329. DOI: 10.1103/PhysRevB.64.085329
6. Jernigan. G. G, Mahadik. N.A, Twigg. M.E, Jackson. E.M, Nolde.J.A. SiGeSn buffer layer for the growth of GeSn films. *J. Appl. Phys.* 2023, 134, 025305. <https://doi.org/10.1063/5.0151479>
7. Zaima. S, Nakatsuka. O, Taoka. N, Kurosawa. M, Takeuchi. W, Sakashita. M. Growth and applications of GeSn-related group-IV semiconductor materials. *Sci. Technol. Adv. Mater.* 2015, 16, 043502. <https://doi.org/10.1088/1468-6996/16/4/043502>
8. Wang. B, Michael. R. H, Harris. T.R, Wallace.P.M, Kouvetakis. K. Enhanced optical and electrical performance of $Ge_{1-x}Sn_x/Ge/Si(100)$ ($x = 0.062$) semiconductor via inductively coupled H₂ plasma treatments. *Semicond. Sci. Technol.* 2019, 34, 045014. DOI 10.1088/1361-6641/ab0916
9. Ghosh. S, Mukhopadhyay. B, Sen. G, Basu. P.K. Performance analysis of GeSn/SiGeSn quantum well infrared photodetector in terahertz wavelength region. *Physica E* 2020, 115, 113692. <https://doi.org/10.1016/j.physe.2019.113692>

10. Ghosh. S, Bhattacharyya. A, Sen.G, Mukhopadhyay. B. Optimization of different structural parameters of GeSn/SiGeSn Quantum Well Infrared Photodetectors (QWIPs) for low dark current and high responsivity. *J. Comput. Electron.* 2021, 20, 1224–1233. <https://doi.org/10.1007/s10825-021-01668->
11. Xu. C, Jiang. L, Kouvetakis. J, Menéndez. J. Optical properties of Ge_{1-x-y}Si_xSn_y alloys with y > x: Direct bandgaps beyond 1550 nm. *Appl. Phys. Lett.* 2013, 103, 072111. <https://doi.org/10.1063/1.4818673>
12. Yamaha. T, Shibayama. S, Asano. T, Kato.K, Sakashita. M, Takeuchi. W, Nakatsuka.O, Zaima. S. Experimental observation of type-I energy band alignment in lattice-matched Ge_{1-x-y}Si_xSn_y/Ge heterostructures. *Appl. Phys. Lett.* 2016, 108, 061909. <https://doi.org/10.1063/1.4941991>
13. S. Wirths et al. Lasing in direct-bandgap GeSn alloy grown on Si. *Nat. Photonics* 2015, 9, 88. <https://doi.org/10.1038/nphoton.2014.321>
14. Fujisawa. T, Arai. M, Saitoh. K. Microscopic gain analysis of modulation doped GeSn/SiGeSn quantum wells: epitaxial design toward high-temperature lasing. *Optics Express* 2019, 27, 2457. <https://doi.org/10.1364/OE.27.002457>
15. Lin. P-H, Ghosh. S, Chang. G-E. Theoretical Analysis of GeSn Quantum Dots for Photodetection Applications. *Sensors* 2024, 24, 1263. <https://doi.org/10.3390/s24041263>
16. Asada. M, A.K. Ama. A.K, Suematsu. Y. Gain and intervalence band absorption in quantum-well lasers. *IEEE J. Quantum Electron.* 1984, 20, 745–753. <https://doi.org/10.1109/JQE.1984.1072464>
17. Chen. Z, Ikonic. Z, Indjin. D, Kelsall. R.W. Design optimization of tensile-strained SiGeSn/GeSn quantum wells at room temperature. *J. Appl. Phys.* 2021, 129, 123102. <https://doi.org/10.1063/5.0042482>
18. Zitouni. O, Saidi. H, Ridene. S. Investigation of α -Sn Dependence of Band Structure and Optical Emission in Si/Si_yGe_{1-x-y}Sn_x/Si Quantum Well Laser. *Silicon* 2024, 16, 3573–3581. <https://doi.org/10.1007/s12633-024-02928-7>